Colloid & Polymer Science Colloid Polym Sci 272:692–703 (1994)

Phase diagrams and phase structure of the *N*-octanoyl-L-glutamic acid oligomer benzyl esters-$CHCl_3$ systems

T. Uehara[1]), H. Hirata[1]), H. Okabayashi[1]), K. Taga[1]), T. Yoshida[1]), and H. Kojima[2])

[1]) Department of Applied Chemistry, Nagoya Institute of Technology, Gokiso-cho, Showa-ku, Nagoya, Japan and
[2]) Gifu National College of Technology, Shinsei-cho, Motosu-gun, Gifu, Japan

Abstract: *N*-Octanoyl-L-glutamic acid oligomer benzyl esters (residue number, $N = 1$–4, 6, 8, and 12) have been synthesized. For the solid samples of $N = 3$–12, x-ray powder diffraction pattern and vibrational spectroscopic measurements have led to the assumption of a β-sheet structure. For the $CHCl_3$-solutions of the *N*-octanoyl tetramers, hexamers, and octamers, the phase diagram consists of three regions (I, II, and III). Region I is an isotropic phase, in which the aggregate structure strongly depends upon concentration, and region II is a lyotropic liquid crystal area. Region III is a two-phase area in which regions I and II coexist. In the case of the trimer solutions, it consists of two regions (I and II). For the oligomers with $N = 3$–12 in region I, it was assumed that micellization induces preferential stabilization of the β-sheet structure depending on the concentration. Further stabilization of the β-sheet structure, was found to occur in region II. For the hexamer, octamer, and dodecamer in $CHCl_3$, results from light-scattering measurements have led to an estimate of the apparent weight-average molecular weights and aggregation numbers of the micelle in region I.

Key words: *N*-octanoyl-L-glutamic acid oligomers – phase structure – β-structure

Introduction

Elliot and Ambrose [1] have discovered that poly-γ-benzyl-L-glutamate (PBLG) takes up an α-helical structure in organic solvents and that a liquid crystalline structure is formed in concentrated solutions. A cholesteric liquid crystalline structure of PBLG solutions has been identified by Robinson et al. [2–4] and Miller et al. [5] and Itou et al. [6, 7] have compared the Onsager [8] and Flory [9] theories with the experimental results for the transition from isotropic solution to liquid crystal in PBLG solutions. Recently, the orientational order of α-helical PBLG in lyotropic liquid crystals has been discussed in detail, using the results from NMR spectroscopy [10–13].

Concentrated solutions of oligopeptides also provide an interesting class of lyotropic liquid crystals. In particular, for γ-benzyl-L-glutamate oligomers in organic solvents, the molecular structures for samples having an average degree of polymerization equal to 3, 4, and 5 have been investigated by the use of viscometric and infrared spectroscopic measurements [14]. γ-Benzyl-L-glutamate oligomers (residue number $N = 4$ and 6), which have C-terminal *o*–nitrophenylthio and N-terminal ethylamide groups, have been synthesized and their aggregate structures in organic solvents have been discussed [15–19]. However, a detailed study of the phase diagram and a theoretical explanation of the observed phase transition in the γ-benzyl-L-glutamate oligomer-organic solvent systems have not yet been made. Moreover, the micellar structure formed by hydrogen bonds still remains unresolved and its further investigation is highly desirable.

For low molecular weight PBLG, a β-structure has been assumed by Blout and Asadourian [20],

and has been studied in detail by analysis of the infrared bands characteristic of the amide CONH group [21–25]. In particular, the amide I and amide II bands of polypeptides have been analyzed with respect to their chain conformation [24, 25].

In the present study, a series of *N*-octanoyl-L-glutamic acid oligomer benzyl esters ($N = 1$–4, 6, 8 and 12) has been synthesized by a stepwise procedure [26, 27], and the conformational study of these oligomers in the solid state has been discussed using the results obtained from the x-ray powder diffraction patterns and the vibrational spectra of these oligopeptides. Further fundamental data have been obtained from phase diagrams, molar volumes, micellar molecular weights, and conformations of these oligomers in $CHCl_3$ for a detailed discussion of the structure of the oligomer micelle.

Experimental

Materials

Octanoyl-L-glutamic acid oligopeptides were prepared by a stepwise procedure as follows. *N*-tert-Butoxycarbonyl-L-glutamic acid α,γ-dibenzyl ester oligomers (BOC-Glu oligomer dibenzyl esters) were prepared from *N*-tert-BOC-L-glutamic acid γ-benzyl ester and L-glutamic acid α,γ-dibenzyl ester toluene *p*-sulfonate in dichloromethane in the presence of triethylamine. The usual 1-ethyl-3-(3-dimethylaminopropyl) carbodiimide (EDC) method [26, 27] was used for the condensation reaction. For the BOC-Glu oligomer benzyl esters thus obtained, confirmation of the residue number (N) was made by proton NMR: the value of N was obtained from the relative peak areas of the ^1H resonance peaks arising from the BOC–CH_3 groups and those of the benzyl protons. The BOC groups of these oligomers were removed by the action of hydrogen chloride in ethyl acetate. The BOC-free oligomer benzyl esters were coupled with the octanoic acid in dichloromethane by the EDC method. The coupling reaction was confirmed by thin-layer chromatography.

The α,γ-dibenzyl esters of *N*-octanoyl-L-glutamic acid oligomer were recrystallized in dichloromethane-ethanol. The samples (residue number, $N = 1$–6) were identified by elemental analysis. The agreement between the calculated and observed values for each atom of these samples was within 0.3%. For the samples of residue number $N = 8$ and 12, identification was made by ^1H NMR.

The residue numbers (N) of the *N*-octanoyl-L-glutamic acid oligomer benzyl esters (octanoyl oligomers), $CH_3(CH_2)_6CO[NHCH(CH_2CH_2CO_2$ benzyl)$CO]_N$O-benzyl, synthesized for the present study were 1, 2, 3, 4, 6, 8, and 12.

For light-scattering measurements, chloroform solutions of these octanoyl oligomers were filtered through an ADVANTEC DISMIC-25JP membrane filter (pore size 200 nm).

Phase diagram determination

Sample solutions were prepared by weighing the octanoyl oligomer and $CHCl_3$ in glass ampoules and the contents were sealed and homogenized by shaking. The temperature dependence of the phase features of the samples was observed by visual inspection as they were held in a temperature-controlled water-bath (rate of temperature elevation and cooling: 0.1 °C min^{-1}). A polarizing microscope (Olympus-pos) with a temperature-variable hot stage was also used to confirm the phase features. The temperature was measured with a digital thermometer (Sato Keiryoki).

Molal volume determination

The apparent molal volumes (Φ_{app}) of the octanoyl oligomer were calculated from the densities of the sample-$CHCl_3$ solutions by using equation (1a)

$$\Phi_{app} = 1/m[(1000 + mM)/\rho - 1000/\rho_S] \quad (1a)$$

$$\Phi_{app} = \Phi^0 + A_V m\,, \quad (1b)$$

where m is the molality of the solution in units of $molkg^{-1}$, M is the molecular weight of the solute, ρ is the density of the solution, and ρ_S is the density of $CHCl_3$. A_V is the experimental slope and Φ^0 is the infinite dilution molal volumes of the solutes. The Φ^0 values were obtained by least-squares fitting of the Φ_{app} values to Eq. (1b). The densities of the sample solutions were measured

with a Lipkin–Davison type pycnometer calibrated with the known density of water. The temperature of the thermostated-bath system was controlled at 298.15 ± 0.02 K.

Light-scattering measurements

Light-scattering measurements were carried out on an Union Giken DLS 700 light-scattering photometer using He-Ne laser light (5 mW) at 632.8 nm. The refractive index increment of the sample solutions was measured on the Union Giken RM-102 differential refractometer at 633 nm. The temperature was kept at 20 ± 0.3 °C by circulating temperature-controlled water through the cell housings. The reduced intensity (R_θ) of light scattered at angle θ from a sample solution (concentration, C in gcm^{-3}) is given by the following equation,

$$R_\theta = R_\theta^0 + KMP(\theta)(C - C_0)\,, \qquad (2)$$

when the external interference is negligible. In this equation, R_θ^0, M, and $P(\theta)$ are the reduced intensity at the critical micelle concentration (C_0), the apparent weight-average molecular weight, and the particle scattering factor, respectively; K is the optical constant:

$$K = 4\pi^2 n_0^2 (\partial n/\partial c)_c^2 \,/\, L_A \lambda^4\,, \qquad (3)$$

where n_0 and $(\partial n/\partial c)_c$ are the refractive index of solvent and the refractive index increment of solution, respectively, measured at wavelength λ, and L_A is Avogadro's number.

Critical micelle concentration determination

The critical micelle concentration (CMC) of the solute in $CHCl_3$ was determined from plots of Φ_{app} vs concentration for samples of residue number $N = 1$, 2, and 3 and from plots of R_{90} vs concentration for samples of $N = 4$, 6, 8, and 12, as listed in Table 1.

X-Ray powder diffraction pattern and infrared spectral measurements

X-ray powder diffraction patterns were obtained by the use of an RAD-RC diffractometer with counter-monochromator (CuK_α, 50 kV, 110 mA). Infrared absorption spectra were

Table 1. The CMC values[a]) (g/cm³), limiting partial molal volumes[b]) (Φ^0, cm³/mol), apparent weight-average molecular weights (M) and aggregation numbers (m) for the octanoyl oligomers (residue number, N) in $CHCl_3$ at 298.15 K.

Residue number (N)	CMC		(g/cm^3)	(wt%)	Φ^0 (cm^3/mol)	M	m
1			31.9×10^{-3}	2.17	406.2	–	–
2			23.1×10^{-3}	1.57	570.2	–	–
3			14.7×10^{-3}	1.00	729.1	–	–
4[c])		1st	11.2×10^{-3}	0.76	896.9	2200[c])	2[c])
		2nd	4.0×10^{-2}	2.74	–	–	–
6		1st	10.0×10^{-3}	0.68	1163.1	19400	12.3
		2nd	3.9×10^{-2}	2.63	–	–	–
8		1st	6.3×10^{-3}	0.43	1558.5	29500	14.8
		2nd	3.9×10^{-2}	2.63	–	–	–
12		1st	1.5×10^{-3}	0.10	2219.6	46800	16.3
		2nd	1.2×10^{-2}	0.82	–	97700	34.1

[a]) For $N = 1$, 2, and 3, the CMC values were determined from plots of the apparent molal volume vs concentration, while the first CMC for $N = 4$, 6, 8, and 12 and the second CMC for $N = 12$ were determined from plots of R_{90} vs concentration. The second CMC for $N = 4$, 6, and 8 was obtained from plots of the ratio of $A_{1625-1629}/A_{1665-1670}$ vs concentration.

The first CMC values can be expressed as a function of residue number (N) by the following equation:

$$CMC = 0.03798\,EXP(-0.2557\,N),\ r(\text{correlation coefficient}) = 0.97957$$

[b]) (± 1.9 cm^3/mol) from scatter in the plots of Φ^0 vs N.

[c]) Although values of R'_{90} ($R'_{90} = R_{90,solution} - R_{90,solvent}$) were very small ($1.10\times10^{-6}$–$5.56\times10^{-6}$), the reproducibility of the data was very good.

recorded on a Perkin-Elmer 1600 Fourier-transform infrared (FTIR) spectrometer (4000–400 cm^{-1}) with the sample dispersed in KBr discs for the solid states and with the sample-$CHCl_3$ solution sandwiched between two NaCl-plate windows (spacer 0.015–1 mm).

Results and discussion

X-Ray powder diffraction patterns and IR spectra of the solid octanoyl oligomers and the β-sheet structure

The x-ray powder diffraction patterns were measured for the octanoyl oligomers in the solid state. A representative powder pattern of the octanoyl dodecamer is shown in Fig. 1. The lattice spacings observed at 4.71 and 15.53 Å can be assigned to the distance between β-sheet type peptide chains and the side-chain spacing, respectively [28]. Reflections characteristic of the β-sheet structure were also observed for the shorter octanoyl oligomers (N = 3, 4, and 6), as listed in Table 2. Therefore, x-ray powder diffraction patterns provide ample evidence that the series of octanoyl oligomers (N = 3, 4, 6, 8, and 12) takes up the β-sheet structure in the solid state.

The FTIR spectra for a series of octanoyl oligomers (N = 1–4, 6, 8, and 12) in the solid state were measured at room temperature and compared with those of simple amide molecules [21, 22], PBLG [29], and polypeptides [24, 25] taking up the β-sheet structure. The IR band frequencies in the regions of 3200–3500 and 1500–1800 cm^{-1} observed for a series of octanoyl oligomers are listed in Table 3. For the octanoyl oligomers of residue number N = 3–12, it was found that the IR spectra can be satisfactorily explained in terms of a β-sheet structure.

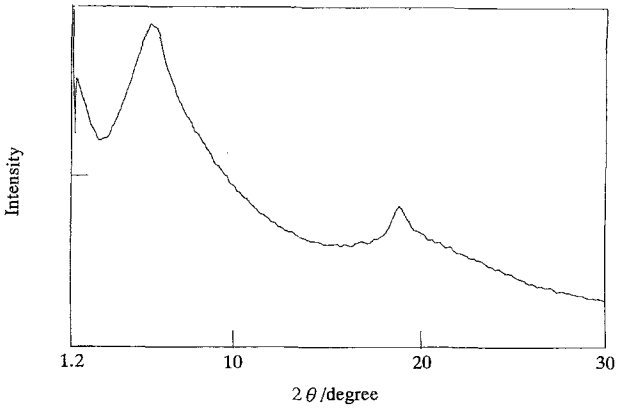

Fig. 1. X-ray powder diffraction pattern of the octanoyl dodecamer.

Table 2. Observed lattice spacings[a]) (Å) characteristics of the β-sheet structure for the octanoyl oligomers (N: residue number).

N = 3	N = 4	N = 6	N = 8	N = 12
15.48 s	16.03 s	15.34 s	15.68 s	15.53 s
4.75 w	4.80 w	4.71 w	4.73 w	4.71 w

[a]) s, strong: w, weak.

The IR bands at 1684–1693 cm^{-1} and 1626–1627 cm^{-1}, observed in common for the octanoyl oligomers (N = 3–12), are assigned to the $\nu(0, \pi)$ and $\nu(\pi, 0)$ amide I vibrational modes of the antiparallel-chain β-form [21, 24, 25]. The amide I split separation ($\Delta\nu$) is as follows: trimer, $\Delta\nu$ = 58 cm^{-1}; tetramer, $\Delta\nu$ = 63 cm^{-1}; hexamer, $\Delta\nu$ = 66 cm^{-1}; octamer, $\Delta\nu$ = 66 cm^{-1}; dodecamer, $\Delta\nu$ = 66 cm^{-1}. That is, as the residue number increases, the split separation approaches that for PBLG until at $N \geq 6$ the values coincide (66 cm^{-1}) [29].

For the antiparallel-chain pleated sheet of synthetic polypeptides and fibrous proteins, the observed frequencies of amide I components are virtually independent of many factors, and are reflected essentially by the properties of the polypeptide backbone structure [30–34]. In the IR spectra of polypeptides and proteins, the $\nu(0, \pi)$ and $\nu(\pi, 0)$ modes for the amide I frequencies are observed at 1685–1705 and 1615–1637 cm^{-1}, respectively, and the mean value of split separation is 67 cm^{-1} [34].

The bands of the octanoyl oligomers (N = 3–12) at 1521–1530 cm^{-1} are due to the amide II vibrational modes characteristic of a β-sheet structure [29].

Thus, the IR bands in the amide I and II regions also provide evidence that the octanoyl oligomers (N = 3–12) take up a β-sheet structure in the solid state.

We have previously investigated [35] the x-ray powder diffraction patterns and vibrational spectra of the octanoyl-L-glutamic acid oligomers

Table 3. Observed IR band frequencies (cm^{-1})[a] of octanoyl oligomers (residue number, N = 1–4, 6, 8, and 12) in the solid state.

Monomer ($N = 1$)	Dimer ($N = 2$)	Trimer ($N = 3$)	Tetramer ($N = 4$)	Hexamer ($N = 6$)	Octamer ($N = 8$)	Dodecamer ($N = 12$)	PBLG	Assignment[b]
3312 vs	3316 vs	3300 sh						
	3286 vs	3282 vs	3289 vs	3289 vs	3288 vs	3290 vs		ν (NH)
		3242 sh						
	1747 s	1743 sh						
		1734 vs	1736 vs	1736 vs	1736 vs	1736 vs	1736 vs	ν $(C=O)_{ester}$
1727 vs	1727 vs							
1725 vs								
1686 vw	1687 vw	1684 m	1689 w	1692 w	1692 w	1693 w	1695 w	
	1665 m	1670 sh	1673 vw	1670 sh	1670 sh	1670 sh		ν $(C=O)_{peptide}$
1640 s	1640 vs	1626 vs	1626 vs	1626 vs	1626 vs	1627 vs	1629 vs	(amide I)
1547 s	1550 sh	1550 sh	1553 sh	1547 sh	1548 sh	1548 sh	1548 s	NH in-plane bending +
–	1534 m	1530 s	1523 s	1522 s	1521 s	1522 s	1524 s	ν (C-N) (amide II)

[a]) s, strong; m, medium; w, weak; v, very; sh, shoulder, and ν, stretching. Only the main vibrational bands are listed.
[b]) The observed band frequencies for the longer octanoyl oligomers (N = 3–12) were assigned by comparison with those for PBLG (refs. [23, 24]) and simple amides (refs. [21, 22]). The band assignment for the monomer and dimer was made by comparison with those for simple amides (refs. [21, 22]).

(acid type, residue number, N = 2–6), and have concluded that the acid-type octanoyl dimer takes up a sheet structure similar to the β_2-conformation of poly-L-glutamic acid [36]. Furthermore, it has been pointed out that the form of the β_2-type sheet structure is promoted by the long acyl chain effect [37].

For the N-octanoyl-L-glutamic acid oligomer benzyl esters, we conclude that the appearance of a β-sheet structure occurs for residue number $N = 3$ and that the β-structure of the trimer is promoted by the close packing of the octanoyl chain [37].

For appearance of an α-helical structure [29] in the solid state, further elongation of the oligopeptide is required, since even the octanoyl dodecamer benzyl ester still takes up a β-structure.

For the monomer and dimer, it seems that amide I splitting (1686–1687 and 1640 cm^{-1}), analogous to that observed for the β-type octanoyl oligomers (N = 3–14), occurs. This band splitting may also be due to the β-like structure (pseudo β-structure) induced by the long acyl chain effect [35, 37].

Phase diagrams of the octanoyl-oligomer-$CHCl_3$ systems

Figure 2 shows the phase diagrams of the octanoyl oligomers (N = 3, 4, and 8)-$CHCl_3$ systems. For the octanoyl trimer-$CHCl_3$ system (Fig. 2[A]), the phase diagram consists of two regions (I and II), while for the other octanoyl oligomer-$CHCl_3$ systems it consists of three regions (I, II, and III) (Fig. 2[B] and [C]). For these phase diagrams, a homogeneous and transparent one-phase solution was obtained in region I, and a homogeneous, turbid, and viscous one-phase solution was obtained in region II. The optically-isotropic property of region I and the lyotropic liquid crystalline state of region II were confirmed under a polarizing microscope. In region III, a two-phase solution system, which has a transparent upper layer and a turbid and viscous lower layer, was obtained. It was also confirmed that the upper layer is optically-isotropic and that the lower layer is in a lyotropic liquid crystalline state. For this region III, the volume percentage of the upper layer decreased linearly and, conversely, that of the lower layer increased with increasing weight-percentage of the sample. This observation is a consequence of the lever rule and proves that the region III system is in equilibrium.

For the octanoyl hexamer-$CHCl_3$ system, the existence of regions I, II, and III was also confirmed, although the phase diagram was not determined.

In the phase diagram of the trimer-$CHCl_3$ system, there is no region in which the isotropic and anisotropic phases coexist. However, for the case

of the tetramer, hexamer, and octamer in $CHCl_3$, the two phases are evidently in equilibrium in region III. Thus, in the octanoyl oligomer-$CHCl_3$ systems, the tetramer is the critical size for coexistence of the two phases. In order to understand the phase separation mechanism in these systems, information on the aggregation number, size, and shape of the oligomer aggregates is required.

In the case of the $CHCl_3$-solutions of the octanoyl monomer and dimer, a homogeneous and transparent one-phase solution was obtained in the concentration region used in this study (below 79 wt % for the monomer and 70 wt % for the dimer), and their optically-isotropic properties were confirmed under a polarizing microscope.

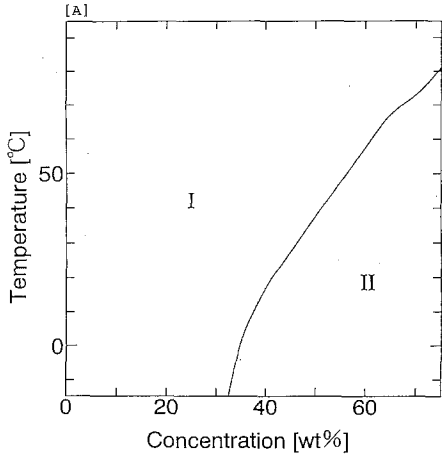

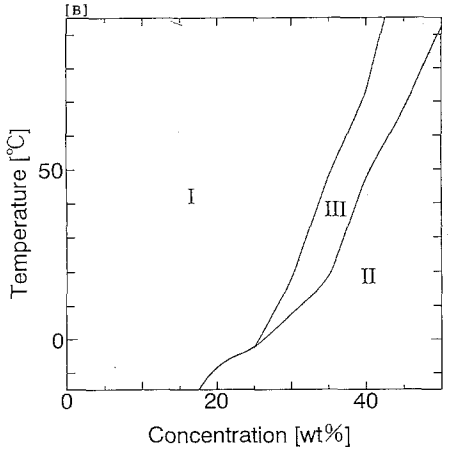

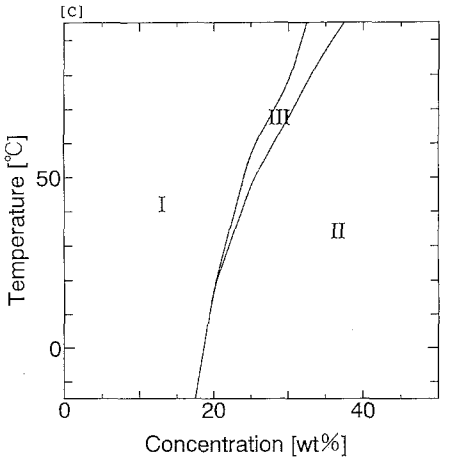

Fig. 2. Phase diagrams of the octanoyl oligomer-$CHCl_3$ systems ([A], trimer-$CHCl_3$; [B], tetramer-$CHCl_3$; [C], octamer-$CHCl_3$). Region I: homogeneous transparent solution; region II: homogeneous turbid and viscous solution; region III: two-phase solution

Molal volumes and micellar molecular weight in $CHCl_3$

For the octanoyl oligomers (N = 1–4, 6, 8, and 12) in $CHCl_3$, the apparent molal volumes (Φ_{app}) of a solute molecule were determined at 298.15 K from density measurements. Figure 3 shows the Φ_{app} values of the octanoyl oligomer solutes at various concentrations above the CMCs. Limiting partial molal volumes (Φ^0) for the solutes in $CHCl_3$ were evaluated from the apparent molal volumes, and are listed in Table 1.

Figure 4 shows the residue-number dependence of the Φ^0 value for a series of octanoyl oligomers in $CHCl_3$, providing the linear relationship ($\Phi^0 = 232.24 + 164.39\ N$) between the Φ^0 value and the residue number (N). The limiting partial molal volume of 164.4 $cm^3\ mol^{-1}$ for the octanoyl and benzyl ester moieties is evaluated by the extrapolation to the intercept.

For longer octanoyl oligomers (N = 4, 6, 8, and 12), light scattering from $CHCl_3$-solutions in region I has been measured at various angles to determine the molecular weight of the octanoyl oligomer micelle. Since no angular dependence of the light scattering was observed, the molecular weight of the micelle was determined from the Debye plots for the 90° direction. The apparent weight-average molecular weights (M) and aggregation numbers (m) of the oligomer micelle are listed in Table 1.

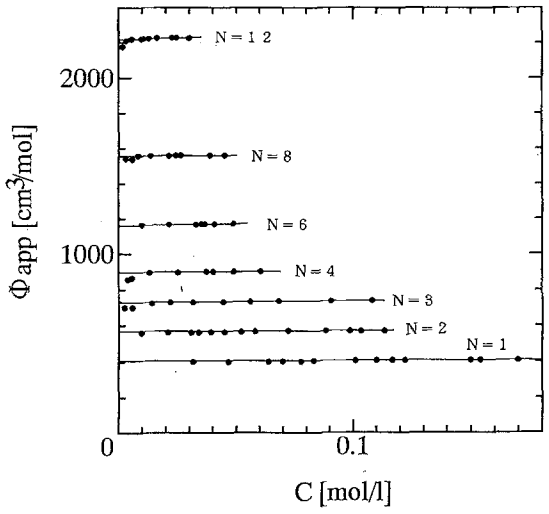

Fig. 3. Apparent partial molal volumes (Φ_{app}) of octanoyl oligomers (residue number N = 1, 2, 3, 4, 6, 8, and 12) in $CHCl_3$ as a function of concentration at 298.15 K

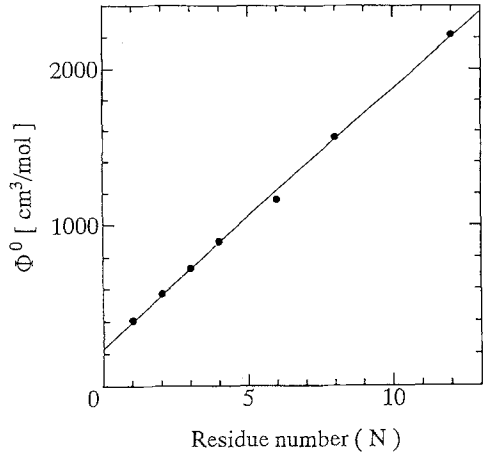

Fig. 4. Residue-number dependence of limiting partial molal volume (Φ°) for the octanoyl oligomers in $CHCl_3$ at 298.15 K

For longer octanoyl oligomers (N = 6, 8, and 12), the apparent weight-average molecular weight of the micelle tends to increase with an increase in residue number. The molecular weight of the tetramer micelle may be very small compared with those for longer octanoyl oligomer micelles, since for the octanoyl tetramer micelle the excess reduced intensities ($R'_{90} = R_{90,\text{solution}} - R_{90,\text{solvent}}$) were very small ($1 \times 10^{-6}$–$6 \times 10^{-6}$ [cm^{-1}]). For the dodecamer-$CHCl_3$ system, a molecular weight of 97 700 was obtained at concentrations greater than the second CMC (1.2×10^{-2} gcm^{-3}, 0.82 wt %), indicating that the size of the dodecamer aggregate changes above this concentration. For the tetramer, hexamer, and octamer, no second CMCs were obtained from plots of R_{90} vs concentration.

A small-angle neutron scattering (SANS) study for the octanoyl oligomer-$CHCl_3$ systems is currently in progress, in order to obtain information on the size and shape of the aggregates. The molal volumes and molecular weights obtained in the present study will be useful for building up a structural model of the octanoyl oligomer micelle for detailed interpretation of the SANS spectra [38].

IR spectra of the octanoyl oligomers in $CHCl_3$ and their conformations

Figure 5 shows the concentration dependence of the IR spectra in the 3200–3500 cm^{-1} region for the very simple octanoyl oligomers (N = 1–3) in $CHCl_3$.

For the octanoyl monomer solutions, the NH stretching bands at 3430 cm^{-1} are observed below the CMC (31.9×10^{-3} gcm^{-3}, 2.17 wt %) (Fig. 5[A]). Even at concentrations below the CMC, no inter-molecular amide-amide hydrogen bonding is detectable at room temperature. The NH stretching band observed at 3424–3430 cm^{-1} should be regarded as the solvent-associated NH stretching.

In fact, it has been confirmed that for N-methylacetamide the non-hydrogen-bonded NH stretching absorption occurs at 3490 cm^{-1} in the gas phase [39, 40]. Therefore, we may assume that the 61 cm^{-1} shift observed in $CHCl_3$ solution results from an interaction of the amide proton with a solvent molecule or an intramolecular ester group.

At concentrations greater than the CMC, the very broad NH stretching band appears at 3300–3380 cm^{-1} in addition to the 3424–3430 cm^{-1} band, and increases in intensity with an increase in concentration (Fig. 5[A]). Furthermore, new strong and broad bands at 3328 and 3366–3368 cm^{-1} appear, and are assigned to the NH stretching vibration arising from two different NH hydrogen bonding modes. Both the intensity and frequency of these NH stretching bands are strongly dependent upon concentration. In the extremely concentrated

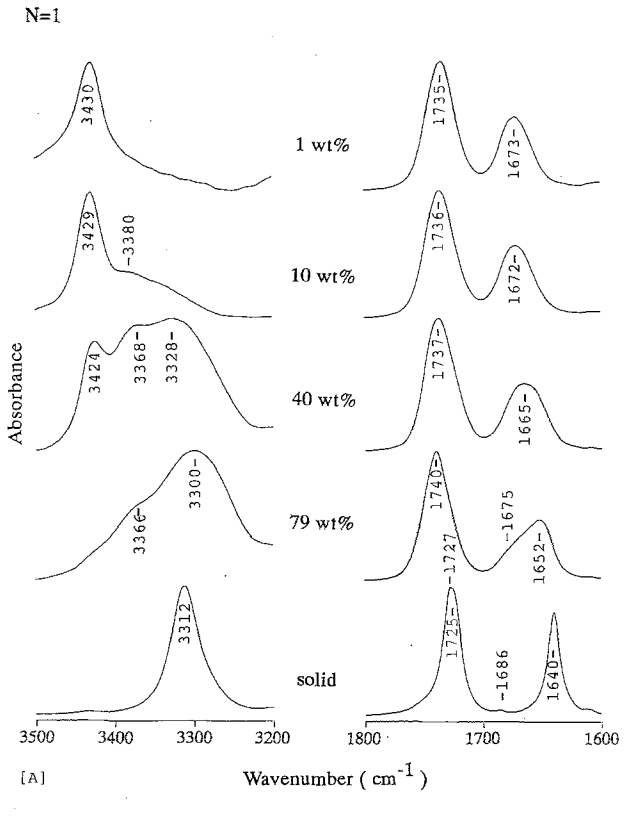

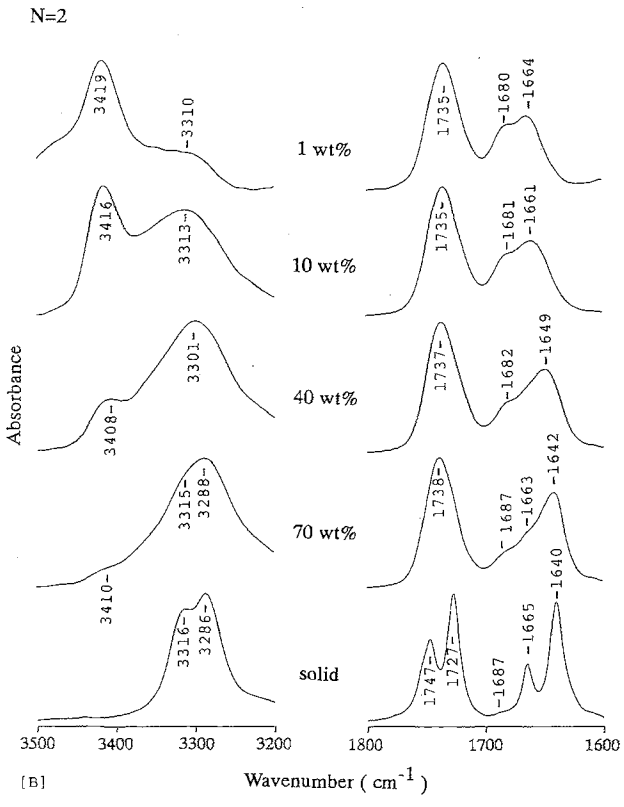

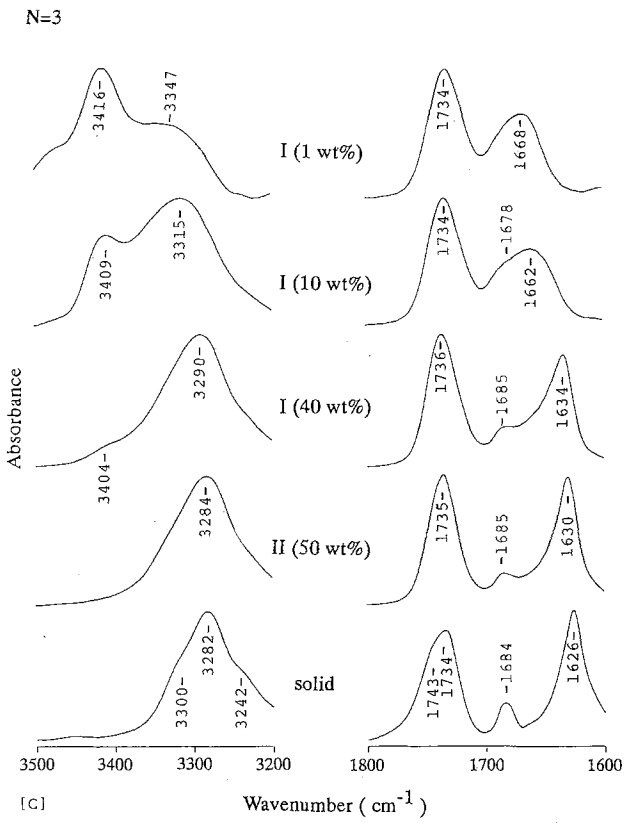

Fig. 5. Concentration dependence of the IR spectra in the 1600–1800 and 3200–3500 cm^{-1} regions for simple octanoyl oligomers (N = 1–3) in $CHCl_3$ ([A], monomer; [B], dimer; [C], trimer)

solution (79 wt %), bands at 3300 and 3366 cm^{-1} are observed in addition to the very weak band at 3430 cm^{-1}. The band at 3300 cm^{-1} is predominant in intensity and is very close in frequency to that (3312 cm^{-1}) of the solid octanoyl monomer.

Such a variation in the NH stretching mode indicates that aggregation of the octanoyl monomer in $CHCl_3$ occurs through formation of hydrogen bonding.

The aggregation of the monomer molecules results in a marked shift of an amide I mode to lower frequency. Below the CMC, the amide I mode appears at 1673 cm^{-1} (Fig. 5[A]). However, in the concentrated solution (79 wt %), the amide I bands are observed at 1652 and 1670–1680 cm^{-1}, and the amide I spectral feature comes close to that of the monomer in the solid state. The marked shift of the amide I mode is the probable result of formation of strong intra- and inter-molecular hydrogen bonds between the amide NH and C=O groups.

For the octanoyl dimer solutions, the concentration dependence of the NH stretching band is pronounced in both frequency and intensity (Fig. 5[B]). Below the CMC a strong band at 3419 cm^{-1} and a very broad band at ca. 3310 cm^{-1} appear. However, at a concentration (70 wt %) greater than the CMC, bands at 3288 and 3315 cm^{-1} and a weak band at 3410 cm^{-1} are observed, and these NH stretching bands are very similar in frequency to those of the solid sample, indicating that the intra- and intermolecular hydrogen-bonding networks formed by the NH groups in the concentrated solution and in the solid are in a very comparable environment.

In the amide I region, two bands at 1664 and 1680 cm^{-1} are observed in a dilute solution (concentration below the CMC) of the octanoyl dimer (Fig. 5[B]). However, in the concentrated solution (70 wt %) there are three bands at 1642, 1663, and 1687 cm^{-1}, which closely correspond to the bands at 1640, 1665, and 1687 cm^{-1}, respectively, for the solid sample. The split separation between the 1642–1664 and 1680–1682 cm^{-1} bands gradually increases with an increase in concentration until, finally, it is comparable with that observed for the solid sample (Fig. 5[B]).

The observations for the IR spectra of the octanoyl monomer and dimer solutions indicate that structures similar to those in the solid state are formed in solutions, but that they are concentration-dependent.

For the octanoyl trimer-$CHCl_3$ solutions, we also found that the concentration dependence of the IR spectra is very similar to that of the monomer and dimer solutions in the NH stretching and amide I regions (Fig. 5[C]). At a concentration equal to that of the CMC (14.7×10^{-3} gcm^{-3}, 1.00 wt %), a very broad amide I band is observed at 1668 cm^{-1}. However, this band gradually shifts to lower frequency with an increase in concentration. Moreover, splitting of the amide I band occurs with further increase in concentration and the split separation ($\Delta\nu$) increases with increasing concentration: $\Delta\nu = 34$ cm^{-1} at 20 wt % and $\Delta\nu = 51$ cm^{-1} at 40 wt %. In particular, it should be emphasized that the spectral feature of the octanoyl trimer solution in region II is extremely similar to that of the solid trimer. In fact, the $\Delta\nu$ value of the amide I-splitting for the trimer solution (50 wt %) in region II is 54 cm^{-1}, and is very close to that for the solid sample (58 cm^{-1}). Such an amide I-splitting pattern reveals that the trimer molecules take up a β-sheet structure similar to PBLG in concentrated region I and in region II.

The amide I band at 1668 cm^{-1}, observed for diluted solutions in region I, may be assigned to the disordered structure [25]. Therefore, for region I the disordered structure is predominant at concentrations below the CMC, but above this value the formation of the aggregates induces preferential stabilization of the β-sheet structure. In region II, we may expect further stabilization of the β-sheet structure to occur.

For the $CHCl_3$-solutions of the longer octanoyl oligomers ($N = 4$, 6, 8, and 12) in region I, the concentration dependence of the IR spectra was investigated in detail. At concentrations below the CMC, the amide I bands are observed at 1665–1670 cm^{-1} in common for these oligomers and are predominant in intensity (spectra not shown, since the spectral features are very similar to that for the trimer, Fig. 5[C]). However, as the concentration increases above the CMC, the amide I band at 1665–1670 cm^{-1} becomes broader until it finally splits into three bands (1625–1629, 1665–1670, and 1689–1693 cm^{-1}). With a further increase in concentration, the two bands at 1625–1629 and 1689–1693 cm^{-1} increase in intensity, while the 1665–1670 cm^{-1} band decreases in intensity. The bands at 1625–1629 and 1689–1693 cm^{-1} are characteristic of a β-sheet structure [24, 25, 29], indicating the preferential

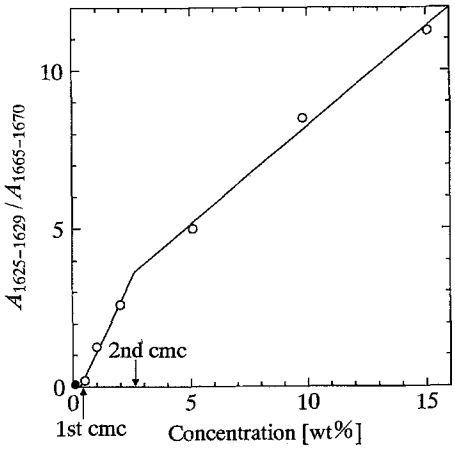

Fig. 6. Relative absorbance ($A_{1625-1629}/A_{1665-1670}$) as a function of concentration in region I for the octanoyl-oligomer-$CHCl_3$ system at 298.15 K. The filled circle shows the relative absorbance below the first CMC

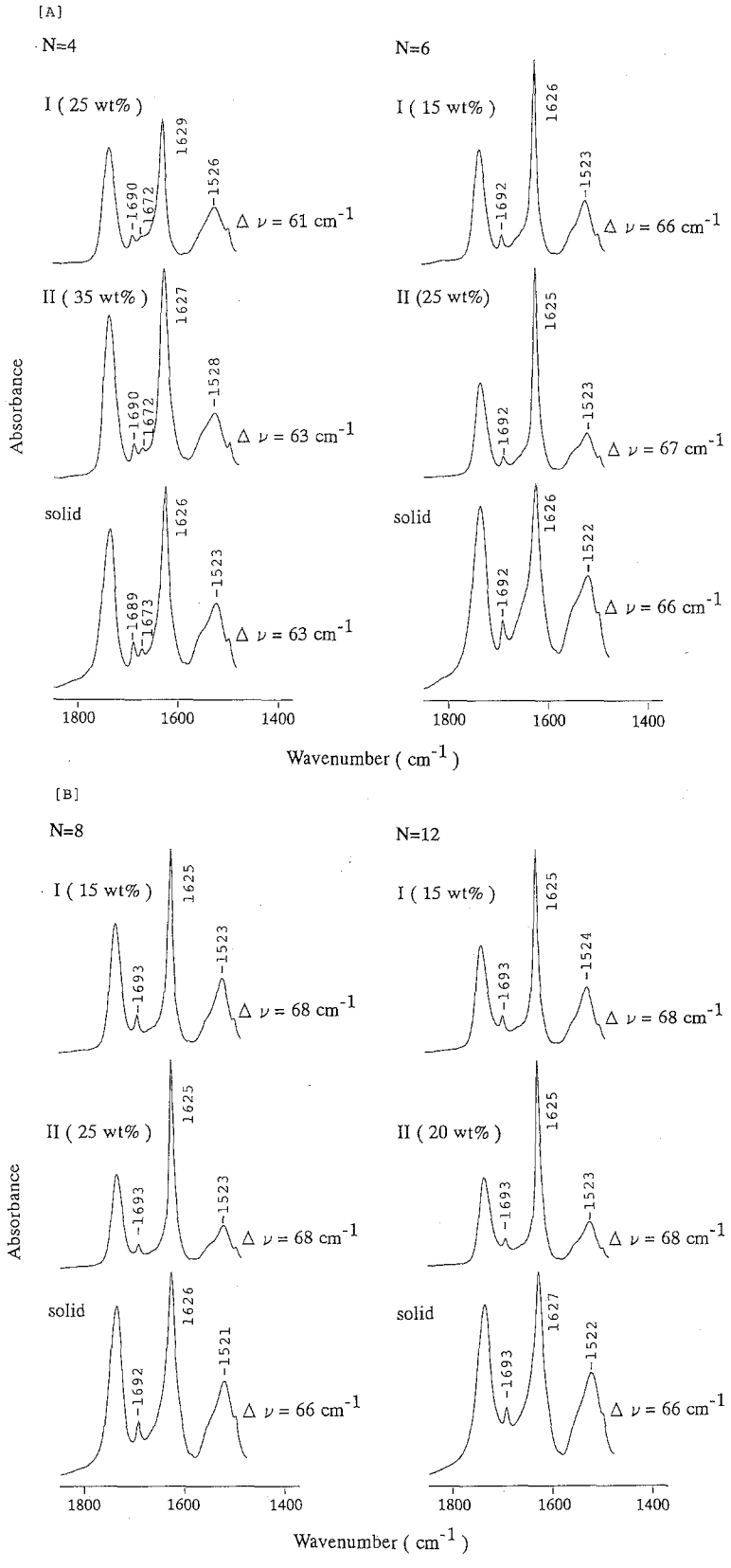

Fig. 7. IR spectra (1500–1800 cm^{-1} region) for the longer octanoyl oligomers ([A], $N = 4$ and 6; [B], $N = 8$ and 12) in region I (concentrated solutions), region II and in the solid state

stabilization of this structure upon micellization. Thus, for the longer octanoyl oligomer solutions, in region I, the conformation of an oligomer molecule is strongly dependent upon the concentration.

Figure 6 shows plots of the relative absorbance ($A_{1625-1629}/A_{1665-1670}$) vs concentration in region I for the octamer-$CHCl_3$ system. As the concentration increases beyond the first CMC, the relative absorbance increases linearly. However, the slope in the plots changes markedly at concentrations greater than 2.63 wt %, which can be regarded as the second CMC. For the tetramer- and hexamer-$CHCl_3$ systems, a similar observation was made. The second CMCs obtained from plots of the ratio of $A_{1625-1629}/A_{1665-1670}$ vs concentration are also listed in Table 1.

It has already been confirmed for surfactant solutions that the size and shape of a micelle change above the second CMC [41]. Therefore, we may assume for the octanoyl oligomer micelle that such a variation in the aggregate state induces further stabilization of the β-sheet structure above the second CMC.

The concentration range between the first and second CMCs corresponds well to that in which the light-scattering measurements were made. In this concentration range, the ratios of $A_{1625-1629}/A_{1665-1670}$ are small compared with those above the second CMC. This reveals that the extent of stabilization of the β-structure is less preferred for these smaller micelles.

Figure 7 shows the IR spectra in the amide I and II regions for the longer octanoyl oligomers ($N = 4$, 6, 8, and 12) in concentrated region I, region II and in the solid state. The amide I-split separations ($\Delta\nu$) are also inserted in Fig. 7. When we compare the $\Delta\nu$ values observed in regions I (concentrated solution) and II and in the solid sample, the split separations are found to be almost identical. This observation shows that a β-sheet structure very similar to that occurring in the solid state is also formed in region II as well as in the concentrated region I.

The IR spectra in the NH stretching region for solutions of these samples in concentrated region I and in region II were compared with those of the solid samples. In solutions, NH stretching bands were observed at 3284–3288 cm^{-1} and these band frequencies were almost identical with those for the solid samples (3288–3290 cm^{-1}). Therefore, we may assume that NH hydrogen-bonding systems, similar to those for the solid samples, are formed in concentrated region I and in region II. For these peptide linkages to be formed the longer octanoyl oligomer solutions must have a highly organized structure under these experimental conditions.

The marked difference between the I and II regions must be in the ordering of the oligomer molecules as well as in the size and shape of the aggregate. In the present study, we cannot discriminate between region I and II by IR spectroscopy. Further investigation by polarized IR and deuterium NMR spectroscopic methods is desirable.

For α-helical PBLG in solution, quantitative studies of the order parameter (s) have been reported. For the magnetically orientated liquid crystalline solutions of PBLG in dioxane, it has been found by x-ray diffraction that the s value is strongly dependent on the concentration [42]. In particular, much attention is now being devoted to the determination of s in lyotropic systems, since comparison may be made with theoretical prediction. Very little is known about the order parameter of the γ-benzyl-L-glutamate oligomers in the lyotropic liquid crystal. For the octanoyl oligomer molecules in the lyotropic liquid crystalline state, further work is also required along these lines.

Conclusion

Results from x-ray powder diffraction patterns and IR spectra have shown that the octanoyl oligomers ($N = 3$, 4, 6, 8, and 12) in the solid state adopt a conformation similar to that of the β-structure of PBLG. The phase diagrams for these oligomers in $CHCl_3$ have been determined. For the trimer, the phase diagram consists of region I (isotropic phase) and region II (lyotropic liquid crystalline phase). However, in the phase diagrams of the tetramer, hexamer, and octamer an additional two-phase area (region III) was found, in which the isotropic phase (upper layer) and the lyotropic liquid crystalline phase (lower layer) coexist.

For a series of oligomers ($N = 1$–4, 6, 8, and 12), in region I, the apparent molal volumes (Φ_{app})

of a solute molecule were determined from density measurements at 298.15 K, and limiting partial molal volumes for the solutes were evaluated. Furthermore, for the longer oligomers ($N = 4$, 6, 8, and 12) in $CHCl_3$, the apparent weight-average molecular weights and aggregation numbers of the micelles were assumed by light-scattering in region I. In particular, for the dodecamer in region I, the molecular weight of the micelle was found to increase above the second CMC.

For the oligomers ($N = 3$–12) in region I, results from IR spectra have indicated that a disordered structure is predominant at concentrations below the CMC and that micellization induces preferential stabilization of a β-sheet structure. For the tetramer, hexamer, and octamer in region I values for the second CMCs were obtained from plots of the ratio of $A_{1625-1629}/A_{1665-1670}$ vs concentration and further stabilization of the β-structure was found to occur at concentrations greater than the second CMC. In region II, an extreme stabilization of the β-sheet structure was also found to occur.

Acknowledgment

We express gratitude to Prof. Charmian J. O'Conner (University of Auckland, Department of Chemistry, New Zealand) for reading the manuscript prior to publication and making suggestions for its revision.

References

1. Elliott A, Ambrose EJ (1950) Disc Farad Soc 9:246–251
2. Robinson C (1956) Trans Farad Soc 52:571–592
3. Robinson C, Ward JC (1957) Nature 180:1183–1184
4. Robinson C, Ward JC, Beevers RB (1958) Disc Farad Soc 25:29–42
5. Miller WG, Rai JH, Wee EL (1974) In: Johnson JF, Porter RF (eds) "Liquid Crystals and Ordered Fluids" Plenum, New York vol. 2 pp 243–255
6. Itou T, Teramoto A (1984) Macromolecules 17:1419–1420
7. Itou T, Teramoto A (1984) Polym J 16:779–790
8. Onsager L (1947) Ann N Y Acad Sci 51:627–659
9. Flory PJ (1956) Proc R Soc A234:73–89
10. Mirau PA, Bovey FA (1986) J Am Chem Soc 108:5130–5134
11. Yamazaki T, Abe A (1987) Polym J 19:777–780
12. Abe A, Yamazaki T (1989) Macromolecules 22:2138–2145
13. Abe A, Yamazaki T (1989) Macromolecules 22:2145–2149
14. Imae T, Ikeda S (1973) Biopolymers 12:1203–1221
15. Okahashi K, Ikeda S (1979) Biopolymers 18:2105–2113
16. Ikeda S, Okahashi K (1979) Biopolymers 18:2115–2126
17. Imae T, Okahashi K, Ikeda S (1981) Biopolymers 20:2553–2566
18. Imae T, Ikeda S (1984) Biopolymers 23:2573–2586
19. Imae T, Ikeda S (1985) Biopolymers 24:585–599
20. Blout ER, Asadourian A (1956) J Am Chem Soc 78:955–961
21. Miyazawa T, Shimanouchi T, Mizushima S (1956) J Chem Phys 24:408–418
22. Miyazawa T, Shimanouchi T, Mizushima S (1958) J Chem Phys 29:611–616
23. Ambrose EJ, Elliott A (1950) Proc Roy Soc [London] Ser A205:47–60; Elliott A (1954) Proc Roy Soc [London] Ser A221:104–114
24. Miyazawa T (1960) J Chem Phys 32:1647–1652
25. Miyazawa T, Blout ER (1961) J Am Chem Soc 83:712–719
26. Hashimoto A, Aoyagi H, Izumiya N (1980) Bull Chem Soc Jpn 53:2926–2928
27. Uehara T, Okabayashi H, Taga K, Yoshida T, Kojima H (1991) J Chem Soc Faraday Trans 88:3451–3459
28. Imae T, Ikeda S (1981) Mol Cryst Liq Cryst 65:73–84
29. Masuda Y, Miyazawa T (1967) Macromol Chem 103:261–267
30. Suzuki S, Iwashita Y, Shimanouchi T, Tsuboi M (1966) Biopolymers 4:337–350
31. Itou K, Shimanouchi T, Oya M (1969) Biopolymers 7:649–658
32. Blout ER, Lenormant H (1957) Nature 179:960–963
33. Lenormant H, Baudras A, Blout ER (1958) J Am Chem Soc 80:6191–6195
34. Chirgadze Yun, Nevskaya NA (1976) Biopolymers 15:607–625
35. Uehara T, Okabayashi H, Taga K, Yoshida T, Kojima H, Nishio E (1993) Bull Chem Soc Jpn 66:2196–2203
36. Itoh K, Foxman BM, Fasman GD (1976) Biopolymers 15:419–455
37. Okabayashi H, Ohshima K, Etori H, Debnath R, Taga K, Yoshida T (1990) J Chem Soc Faraday Trans 86:1561–1567
38. Sheu EY, Chen S-H, Huang JS (1987) J Phys Chem 91:3306–3310
39. Venkatachalapathi YV, Mierke DF, Taulane JP, Goodman M (1987) Biopolymers 26:763–773
40. Gellman SH, Dado GP, Liang G-B, Adams BR (1991) J Am Chem Soc 113:1164–1173
41. Mattoon RW, Stearns RS, Harkins WD (1947) J Chem Phys 15:209–210
42. Murthy NS, Knox JR, Samulski ET (1976) J Chem Phys 65:4835–4839

Received April 21, 1993;
accepted July 27, 1993

Authors' address:

Dr. Hirofumi Okabayashi
Department of Applied Chemistry
Nagoya Institute of Technology
Gokiso-cho, Showa-ku, Nagoya 466, Japan